D. Kuscer et al, Sensors and Actuators A, Volume 366, 1 February 2024, 114946

An advanced miniature fluidic system in multilayer ceramic technology with precise temperature and flow control for *in situ* pollution monitoring

Danjela Kuscer[1,2*], Barbara Repič[1,2], Kostja Makarovič[1,4,5], Maksimiljan Dekleva[3], Gregor Marolt[3], Helena Prosen[3], Darko Belavič[1]

[1]Jožef Stefan Institute, Electronic Ceramics Department, Jamova cesta 39, Ljubljana, Slovenia

[2]Jožef Stefan International Postgraduate School, Jamova cesta 39, Ljubljana, Slovenia

[3] University of Ljubljana, Faculty of Chemistry and chemical technology, Večna pot 113, Ljubljana, Slovenia

4 KEKO-Oprema d.o.o., Grajski trg 15, Žužemberk, Slovenia

5 CoE NAMASTE, Jamova cesta 39, Ljubljana, Slovenia

*corresponding author: danjela.kuscer@ijs.si

Abstract

Rapid, on-site, water-quality monitoring is necessary to prevent and remediate environmental pollution. This study aims to develop a miniature, portable, fluidic system (MFS) designed for the easy insertion of disposable, screen-printed electrodes (SPEs) and the measurement of an electrochemical response (EC) under controlled temperature and flow conditions. The three-dimensional MFS, realised in low-temperature, cofired ceramic and multilayer ceramic technology, consist of three distinct cavities, each with separate inlet and outlet channels. These channels are designed to maintain an equivalent flow rate across all three cavities. The MFS allows simultaneous measurements at three measuring sites, temperature control of the fluid from room temperature to 125 °C via integrated heaters and temperature sensors, and flow regulation up to 20 mL/min via an external fluid pump. The EC values obtained from the SPEs in a standard solution of potassium ferrocyanide/potassium ferricyanide at room temperature and under stagnant conditions were consistent with measurements conducted in the MFS, droplet and conventional electrochemical cells, confirming the accuracy and reliability of the MFS. The EC response was confirmed in the MFS under flow conditions of 4 mL/min and temperatures of 25 °C, 35 °C, and 45 °C. This shows that multilayer ceramic technology enables the fabrication of a miniature, three-dimensional MFS with integrated fluidic and electronic components that provide reliable and accurate electrochemical measurements using a commercial SPE under controlled flow and temperature conditions.

Keywords: miniaturized fluidic system, multilayer ceramic technology, LTCC, temperature and flow control, electrochemistry, monitoring.

1 Introduction

The economic development of a population through industrialisation, agricultural production and urban life is accompanied by ecological challenges in the form of pollution. The pollution of water with chemicals, nutrients or bacteria presents a risk to human health, both directly through drinking and indirectly through the contamination of food. Water-quality monitoring is, therefore, important to identify water-quality problems and develop targeted programmes to prevent pollution and enhance remediation [1].

Typical techniques for water monitoring are high-performance liquid chromatography and mass spectrometry. In this way the information obtained about the pollutants' concentration in the sample is accurate, reliable, and comes with a low detection limit for the selected substance. However, the procedure is time-consuming and needs to be carried out in laboratories by highly skilled personnel with expensive

equipment, which is the key limitation for the real-time analysis of water in remote locations and in developing countries [2,3].

Several studies have reported on miniature, microfluidic electrochemical sensors consisting of a working electrode (WE), a counter electrode (CE) and a reference electrode (RE) with appropriate electrical connections integrated into or placed inside a housing with microchannels [4–8]. These sensors have been used to detect various pollutants in water, such as heavy metals [9], nitrates and nitrite ions [10,11], phenolic compounds [12,13], antibiotics [14], pesticides and herbicides [15,16], by measuring the changes in the electrical characteristics such as voltage, current and impedance, resulting from the electrochemical reactions of the molecules on the surface of a working electrode. These studies have consistently found that electrochemical sensors are easy to use and allow the rapid analysis of the target analyte with high sensitivity, and can thus provide both quantitative and qualitative information about the sample [7,17,18].

Miniature fluidic systems (MFSs) are often fabricated from silicon, glass, polymers and paper by soft lithography and laser-writing techniques [6,19,20]. All these materials allow the fabrication of adjustable fluidic structures and the integration of components such as sensors, actuators and electronics. Paper with its porous structure is well suited to biological assays, although making well-defined microchannels is difficult. Silicon and glass can withstand high temperatures, but manufacturing MFSs from these materials is complex, time-consuming and requires expensive materials, hazardous etchants and complex facilities such as clean rooms. Polymers are widely used because of the simple patterning of the fluidic elements and low costs, but integrating electronics into such MFSs is difficult and costly. An interesting alternative to these materials is low-temperature, co-fired ceramic (LTCC) and multilayer ceramic technology (MCT). Ceramic tapes in the green state, each with a specific geometrical pattern and selected with screen-printed electronic components, are laminated and then sintered together at up to 900 °C to form a complex, three-dimensional ceramic structure. The resulting structure is chemically stable in a wide pH range, in solvents such as alcohols, ethers, ketones, and hydrocarbons, has good mechanical properties and can withstand high temperatures up to several hundred °C. LTCC technology is mature, allows for the fabrication of three-dimensional structures with integrated electronic and fluidic components, and thus the MFS's production process is simple and economical [21–24]. For example, Goldbach et al. [25] developed a microfluidic device with integrated electrochemical sensors for the detection of three different phenolic compounds from their mixture. The authors report that a number of factors, including an uneven channel structure and possible leakage of the liquid, affect the detection. Almeida et al. [14] demonstrated the applicability of a similar fluidic device in LTCC technology for the simultaneous detection of two antibiotics from aquaculture water with the limit of detection below 35 μg/mL. Vasudev et al. [26] also realised a microfluidic device in LTCC, but they used a disposable electrochemical sensor for the detection of cortisol. These systems were developed for fluids with a viscosity in the range of a few mPas and enable measurements at room temperature. However, LTCC devices can also be used in areas where high temperatures and contact with aggressive chemicals are common, e.g. in food processing, industrial real-time and environmental monitoring, energy management, aerospace or the automotive industry [27–29].

Although the effective electrochemical detection of various compounds in LTCC-based microfluidic systems was confirmed, insufficient attention has been paid to temperature control, which is important for electrochemical measurements. The oxidation-reduction reactions that take place at the working and counter electrodes depend on the temperature for both the analytes and the electrolytes. This follows from the basic electrochemical relationships, including the Nernst equation, the Randles-Ševčík equation and the Butler-Volmer equation in electrochemical kinetics [30]. For example, the increased (controlled) temperature can be used to accelerate the electrochemical kinetics [31], reduce the activation overpotentials [32] and thus make the electrochemical reaction more favourable and efficient. Another important aspect is the increase in mass transport at high temperatures due to higher diffusion or convection, which often leads to increased Faradic current signals and is particularly useful for increased sensitivity of systems with sluggish kinetics as well as lower detection limits for electroanalytical applications, including sensors [33]. In all the studies mentioned, the response was measured at room temperature in fluids with a viscosity, similar to

water, 1 mPas. Additionally, the continuous, long-term, accurate analysis of the samples requires reliability and stability of the sensor components, in particular reference and working electrodes. This is difficult to achieve with integrated sensor components. The miniature analytical device with temperature and flow control which allow easy placement and replacement of disposable, array-ordered sensors, could be of benefit for the on-site detection of contaminants by screening methods, contributing to a faster environmental pollution assessment and decision making.

We fabricated an advanced, three-dimensional MFS from LTCC and MCT with integrated heaters and temperature sensors for temperature management and an external fluid pump for flow control. The system is designed for operation in a continuous flow from 0.5 to 20 mL/min and in the temperature range between room temperature and 125 °C. The MFS allows simultaneous measurements at three measuring sites and each a different temperature. The electrochemical response in the MFS was evaluated by using disposable, commercially available, screen-printed electrodes (SPEs) and standard solutions of potassium ferrocyanide/potassium ferricyanide (HCF) in a phosphate buffer solution (PBS) using cyclic voltammetry (CV). The functionality of the developed miniature fluidic system was demonstrated by electrochemical measurements in a stationary fluid and a flow regime of 4 mL/min at constant temperatures of 25, 35 and 45 °C.

2 Experimental

2.1 Fabrication of the miniature fluidic system

The MFS was designed as a monolithic ceramic multilayer structure made of commercial LTCC tape with a thickness of ~250 μm (951AX Green Tape, DuPont, Wilmington, DE, USA). To fabricate the cavities and channels, the green tape was perforated with a laser (ProtoLaser S, LPKF, Garbsen, Germany) and a puncher (PAM -8SCC, KEKO equipment, Žužemberk, Slovenia). The electronic components, i.e., heating elements (PTC2611-I, Ferro, King of Prussia, PA, USA), temperature sensors (NTC2114, Ferro, King of Prussia, PA, USA), internal connections (Ag, 6142D, DuPont, Wilmington, DE, USA), and solder contact pads (Ag-Pd, 6146, DuPont, Wilmington, DE, USA) were fabricated using thick-film pastes applied to the unfired LTCC tape with a screen printer (C1010, Aurel, Modigliana, Italy). Each layer was air dried in a ventilated oven at 120 °C for 15 min. The structure consisted of 22 green tapes assembled in three stacks. Each stack was isostatically laminated at 20 MPa and 70 °C for 10 min. They were then brought together and uniaxially laminated at 5 MPa and 50 °C for 10 min. The laminated structure was heated to 450 °C in a chamber furnace (PEO603, ATV Technologie, Vaterstetten, Germany) for 60 min at a heating rate of 7 °C/min. The temperature was then raised to 875 °C at a heating rate of 10 °C/min, held for 30 min, and then cooled to room temperature at a rate of 10 °C/min. The inlet and outlet fluidic ports were bonded to the structure using an epoxy adhesive (ES569, Permabond, Winchester, UK). The adhesive was air cured in an oven at 150 °C for 60 min.

2.2 Flow and temperature control

The fluid flow in the MFS was driven by a diaphragm liquid pump (FMM 20 KPDC-P, KNF Freiburg im Breisgau, Germany). The pump was computer controlled by pulses in the frequency range from 1 to 20 Hz. The dispensed volume can be set from 5 to 17 μL with a flow rate of up to 18 mL/min.

The flow of water through the cavity of the MFS was measured at a constant dispensed volume of 5 μL in the frequency range from 1 to 20 Hz. The temperature of the water at inlet position was 22 °C. The relation between pulses' frequency and the flow rate was calculated from the mass of water flowing through the cavity within a period of 5 min, taking into the consideration the density of the water at the selected temperature. The time-dependent flow was measured for 10 min at constant frequencies of 1, 4, 8, 16 and 20 Hz.

The temperature-control system of the MFS was calibrated with a discrete temperature sensor inserted into the MFS's cavities. The temperature sensor was fabricated from an NTC resistor (NTC2114, Ferro, King of Prussia, PA, USA) screen-printed on an alumina substrate (Rubalit 708S, 96% Al_2O_3, CeramTec, Plochingen,

Germany) with dimensions of 34.0 mm × 10.0 mm and a thickness of 0.64 mm using a screen printer (C1010, Aurel, Modigliana, Italy). The electrical contacts were made from a silver-based, thick-film conductor (9912MM, ESL, King of Prussia, PA, USA). The printed layers were dried in a dryer at 120 °C for 15 min and then fired in a chamber furnace (PEO603, ATV Technologie, Vaterstetten, Germany) at 850 °C for 10 min in air with heating and cooling rates of 33 K/min.

For the temperature-control system in the MFS we selected heaters with a linear positive temperature dependence (PTC, Eq (1)) and temperature sensors with a negative temperature dependence (NTC, Eq (2))

$$R_2 = R_1 [1 + \alpha (T_2 - T_1)] \quad (1)$$

$$R_2 = R_1 e^{\beta \left(\frac{1}{T_1} - \frac{1}{T_2}\right)} \quad (2)$$

where R_1 and R_2 are the resistances at temperatures T_1 and T_2, respectively, α is the temperature coefficient of resistance, β is the thermistor constant.

Discrete and integrated temperature sensors and heaters were characterized using a computer-controlled system consisting of an environmental chamber (VCL 7006, Voetsch Industrietechnik, Balingen-Frommern, Germany) and a multimeter (2700, Keithley Instruments, Cleveland, Ohio, USA). A resistance in the temperature range from -25 °C to 125 °C was measured. The resistance at 25 °C, α and β were evaluated based on 40 test samples.

2.3 Electrochemical measurements

Electrochemical studies were carried out using commercial SPEs (C110, Methrom DropSens, Oviedo, Spain), which consist of a carbon working electrode, a counter electrode and a silver quasi-reference electrode deposited on an alumina substrate with a length of 35 mm, width of 10 mm and a thickness of 0.5 mm. The electrodes were connected to a potentiostat-galvanostat (Multi Autolab M204, Methrom, Utrecht, The Netherlands) with a cable connector for the SPE (DRP-CAC 7000047, Metrohm DropSens, Oviedo, Spain). The CV measurements were performed with Nova 2.1.5 software (Metrohm Autolab B. V., Utrecht, The Netherlands) without SPE preconditioning. The SPE was positioned into the MFS's cavity containing ~0.3 ml of deaerated liquid, i.e., an electrolyte containing the electrochemical probe. The electrolyte was a 0.1 M PBS with a pH of 7.0 prepared by dissolving sodium dihydrogen phosphate monohydrate ($NaH_2PO_4 \cdot H_2O$; ≥ 99.0%, Merck, Darmstadt, Germany) and disodium hydrogen phosphate (Na_2HPO_4; anhydrous, > 99.5%, Fluka, Seelze, Germany) in ultra-pure water pre-treated with a water-purification system (Simplicity 185, Millipore, Guyancourt, France). The electrochemical probe was a 0.005 M $[Fe(CN)_6]^{3-}$/$[Fe(CN)_6]^{4-}$ (molar ratio 1:1) in PBS (HCF) prepared by dissolving potassium hexacyanoferrate(II) trihydrate ($K_4[Fe(CN)_6] \cdot 3H_2O$; ≥ 98.5%, Carlo Erba, Val-de-Reuil, France) and potassium hexacyanoferrate(III) ($K_3[Fe(CN)_6]$; anhydrous, ≥ 99% Carlo Erba, Val-de-Reuil, France) in PBS.

Two sets of CV measurements with the SPE and MFS were performed: i) at a constant temperature of 25 °C and flow rates of 0, 1, 2, and 4 mL/min, and ii) at a constant flow rate of 4 mL/min and temperatures of 25, 35, and 45 °C. Reference measurements were performed at 25 °C without any flow using SPE electrodes i) drop-casted with 0.1 mL of liquid covering all three electrodes and ii) immersed in an electrochemical cell filled with 10 mL of electrolyte. A new, unused electrode was used for each measurement setup. CV measurements were made in the potential range between -0.35 V and 0.45 V and between -0.6 V and 0.8 V, against Ag with a scan rate of 100 mV/s. 0.0 V was used as a start potential, which is close to the value of the open-circuit potential (0.16 V). In the first half-cycle, the potential was swept towards the positive switching potential with a step of 0.00244V. Each measurement was stopped after 3 cycles and the results of the second cycle were evaluated. A capacitive current (i_{cap}) in 0.1 M PBS was determined as the difference between the anodic and cathodic current at 0.0 V. The voltammograms obtained for the probe were characterised by a peak current (i_p) and a peak potential (E_p) for both the anodic and cathodic currents. The

ratio of cathodic to anodic peak current (i_{pc}/i_{pa}) and the peak-to-peak potential separation (ΔE_{pp}, Eq (3)) were calculated.

$$\Delta E_{pp} = E_{pa} - E_{pc} \quad (3)$$

3 Results and discussion

3.1 Design and fabrication of MFS and discrete temperature sensor

The MFS was designed as a miniature device that allows control of the liquid flow, heating of the liquid and its temperature regulation in the cavities. The device required the integration of fluidic (channels, cavities) and electronic components (heaters, temperature sensors, electrical interconnections) within a structure so that direct contact between the electronic components and the liquid was prevented. We designed the rectangularly shaped MFS with external dimensions of 64.0 mm × 31.1 mm × 4.5 mm, which consists of three cavities that, in terms of their dimensions, enable a tight fit to commercially available SPEs for electrochemical measurements. The MFS allows for easy replacement of the SPEs in the cavities. For the realization of such a device, we chose multilayer ceramic technology based on LTCC material, which allows the construction of three-dimensional structures with integrated fluidic and electronic components. The layouts of the fluidic and electronic components of the MFS are presented in Figure 1.

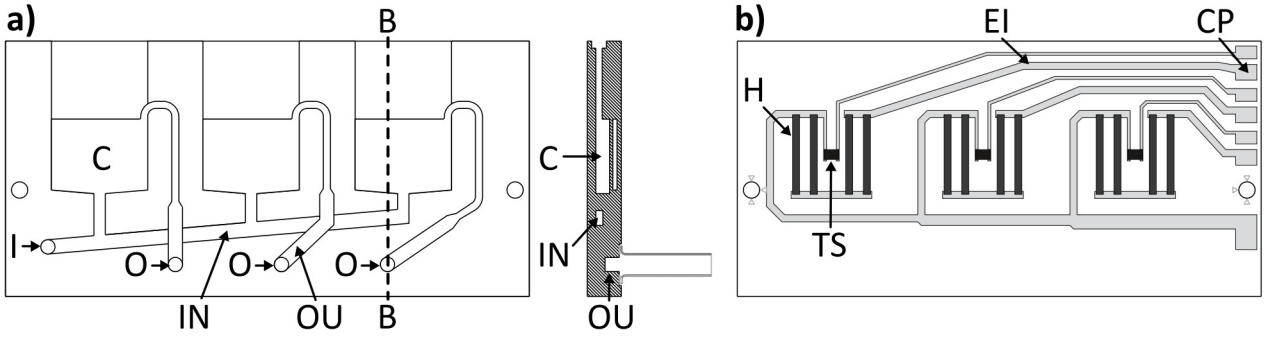

Figure 1: a) Layout of the fluidic components of MFS: C-cavity; IN - inlet channel; OU-outlet channel, inlet port (I) and outlet port (O). Top view on the left and cross-section B-B on the right. b) Layout of the electronic components of MFS: heaters (H), temperature sensors (TS), electrical interconnection (EI), contact pad (CP).

The MFS consists of three cavities, each with a separate inlet (IN) and outlet (OU) channel. The geometry of the cavities provides a similar volume of fluid in all three cavities, while the designed geometry of the channels allows a comparable flow rate through all three cavities. However, when tested at a flow rate of 5 mL/min, a difference of 0.3 mL/min was observed between the flow rates through each cell, mainly due to the different hydrodynamic resistances of the channels. The hydrodynamic resistance of water through cavity 1, 2 and 3 at 25 °C was 350, 353 and 325 MPa·s/m^3, respectively. The values were calculated taking into account the viscosity of the water, the dimensions of the rectangular cross-section of the channels and their length [34]. The details are described in Supplementary material. The design of the channels and cavities also allows for smooth filling and emptying of the liquid and simplified cleaning of the interior (Figure 1a).

To regulate the temperature of the liquid in the MFS, a heater, a temperature sensor and electrical interconnections are integrated into the LTCC structure. The heater and the temperature sensor are placed above each cavity and electrically interconnected with contact pads (Figure 1). The geometry of the heater is designed to provide a homogeneous temperature distribution in the cavity, and the temperature sensor is positioned in the centre of the cavity.

Three separate stacks of green LTCC tapes are shown in Figure 2. The first stack (Figure 2a) with patterned IN and three cavities (C) is placed at the bottom. The second stack shown in Figure 2b, consists of IN and OU,

three C as well as an I port. This stack is covered by the third stack (Figure 2c), devoted to electrical components and consists of an LTCC tape with screen-printed components for temperature control. The I and O ports are also visible. Note that the electrical connections to contact pads are not seen since they are covered by LTCC tape. This stack is covered by LTCC tape, which prevents the contact of liquid with the electrical components (not shown in this Figure). The top view and C-C cross-section images of the laminated and fired MFS are shown in Figure 3.

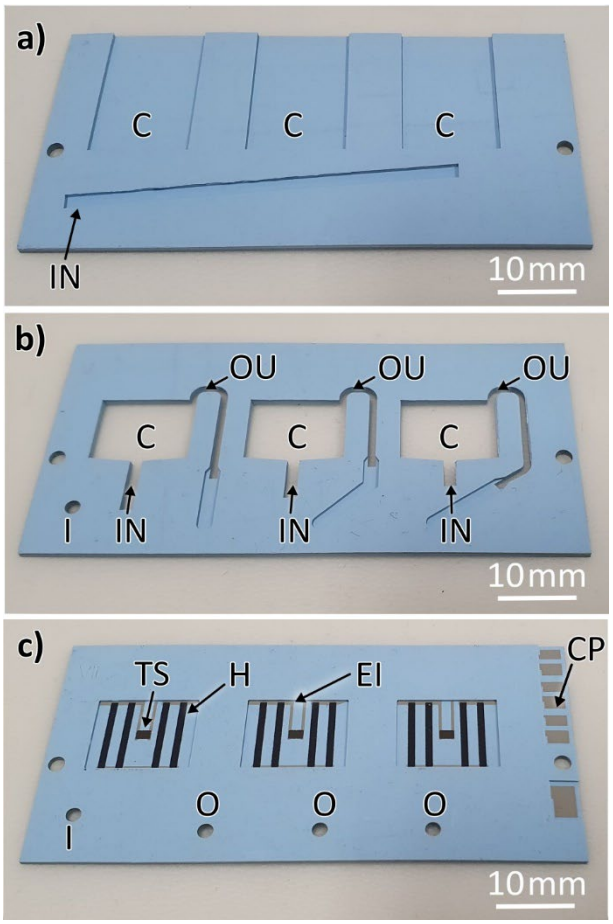

Figure 2: Patterned green LTCC stacks before lamination. a) LTCC stack with inlet channel (IN) and three cavities (C); b) stack with discrete inlet (IN) and outlet (OU) channels, three cavities (C) and inlet (I) port; c) stack with screen-printed heaters (H), temperature sensors (TS), electrical interconnections (EI), contact pads (CP), inlet port (I) and three outlet (O) ports.

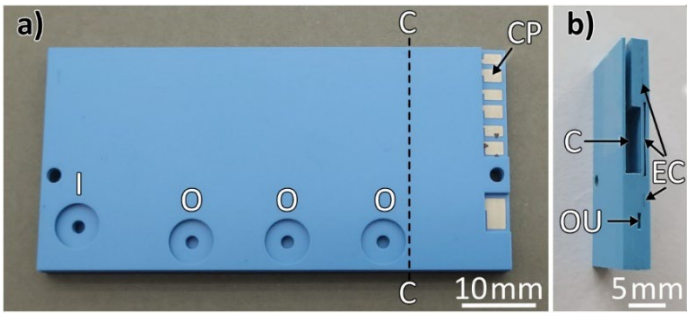

Figure 3: Fired MFS realised in LTCC technology. a) Top view and b) cross-section in C- C. I- inlet port, O - outlet port, CP - contact pads, C - cavity, OU - outlet channel, EC - electronic components (heaters and temperature sensors).

3.2 Flow in the miniature fluidic system

The flow in the MFS as a function of frequency, and the time-dependent flow over 10 min are shown in Figure 4a and b, respectively.

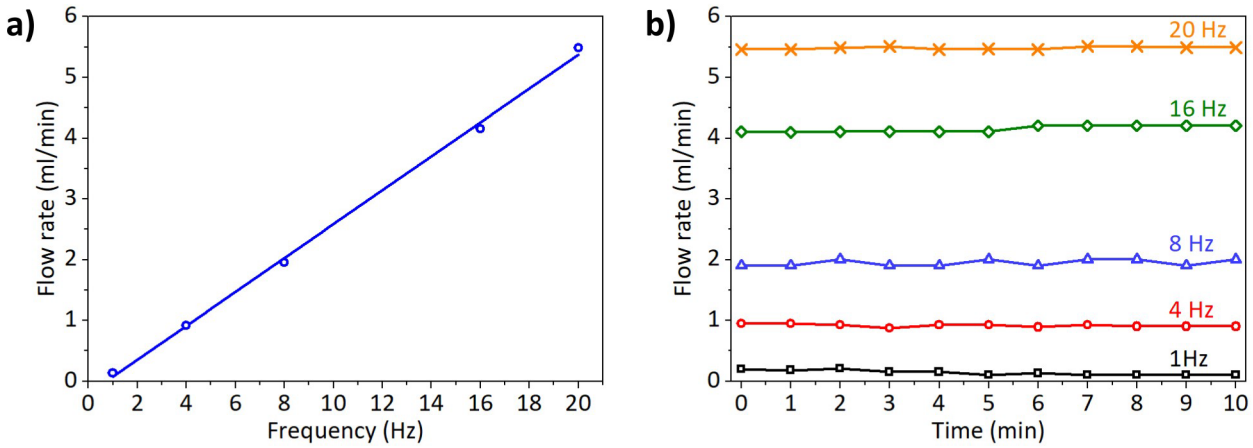

Figure 4: a) Flow of water as a function of fluidic pump pulse frequency at 22 °C. b) Time-dependent flow of water at frequencies of 1 (open square), 4 (open circle), 8 (open triangle), 16 (open diamond) and 20 Hz (cross).

Figure 4a shows a linear correlation between the fluidic pump pulse frequency and the flow. When the frequency increased from 1 to 20 Hz, the flow rate increased from 0 to 6 mL/min. At frequencies of 1, 4, 8, 16, and 20 Hz the flow rates are 0.14 ± 0.04, 0.92 ± 0.04, 1.95 ± 0.05, 4.15 ± 0.05 and 5.48 ± 0.02 mL/min, respectively (Figure 4b). These results demonstrate the stability of the flow rate over a period of 10 min with the standard deviation in the range between 0.02 and 0.05 mL/min. In contrast to Goldbach et al. [25], we did not observe any leakage problems.

3.3 Characterisation of heaters and temperature sensors

A thick-film resistor with a positive temperature dependence (PTC) that acts as a heater (H) was evaluated. Figure 5 shows the resistivity versus temperature in the range from -25 °C to 125 °C for the heater integrated into the LTCC structure. Its resistivity increased with the temperature and showed a linear response. The heater was capable of reaching 125 °C. They were characterised by a resistance of 39 ± 3 Ω at 25 °C and a temperature coefficient of resistance (α) of 2650 ± 60 10^{-6}/K.

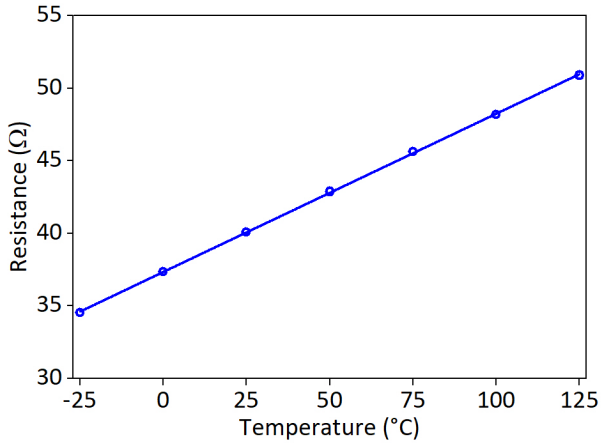

Figure 5: Resistivity-temperature curves measured from -25 °C to 125 °C for heaters integrated into miniature fluidic system.

Temperature control of the liquid in the MFS is accomplished by a resistor with a negative temperature dependence (NTC) that acts as a temperature sensor (TS). The TSs were integrated into the LTCC structure (integrated TS) and on an alumina substrate (discrete TS). The resistance versus temperature measured from -25 °C to 125 °C for the integrated and discrete TSs are shown in Figure 6a and b, respectively. Their resistivity decreased with the increasing temperature. For the integrated TS a resistance of 12000 ± 250 Ω at 25 °C and a thermistor constant (β) value of -2400 ± 50 K was obtained. The resistance of 9800 ± 200 Ω at 25 °C and a thermistor constant (β) of -2450 ± 50 K were measured for the discrete TS. We measured a lower resistivity and a slightly higher β for the discrete TS even though the discrete and integrated TSs were made of the same thick-film paste. The different characteristics of the resistors originate from the different substrates and different firing conditions. The discrete TS on the alumina substrate was fired at 850 °C for 10 min while the integrated TS on the LTCC was fired at 875 °C for 30 min. Hrovat el at. [35] showed that the thick-film paste NTC2114 and the LTCC chemically interact at elevated temperatures, while interactions with Al_2O_3 have not been observed. LTCC contains glass, and SiO_2 from the glass diffuses into the resistor, which increases its resistivity and the thermistor constant.

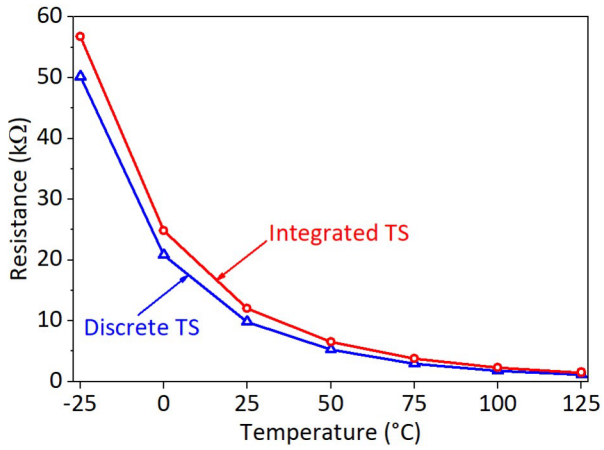

Figure 6: Resistivity-temperature curves for discrete (open triangle) and integrated temperature sensors (open circle) measured from -25 °C to 125 °C.

Temperature control of the liquid in the MFS is accomplished with an integrated H and TS in the LTCC structure above each cavity. The TS measures the temperature of the LTCC wall above the cavity and, together with external electronics, allows control of the power supply to the H. The TS and H of each cavity are controlled separately, allowing independent temperature control of the liquid in each cavity. The temperature measured by the integrated TS does not correspond to the actual temperature of the liquid in the cavity. Therefore, to resolve this discrepancy, the temperature of the water in the cavity was measured with a discrete TS inserted into the cavity of MFS filled with water (Figure 7a). The temperature measured with integrated TS sensor and discrete TS as a function of supply voltage is shown in Figure 7b.

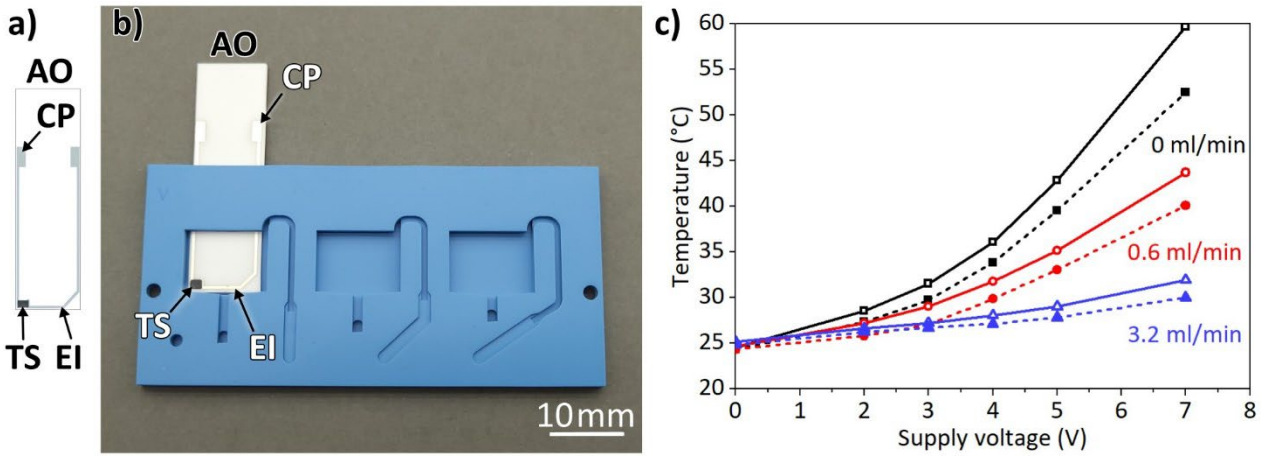

Figure 7: a) Layout of discrete TS. b) Discrete TS inserted into open MFS; AO - alumina substrate, EI – electrical interconnections, CP – contact pads; b) temperature of the liquid measured by discrete (dashed lines) and integrated TS (solid lines) at a flow of 0 (square), 0.6 (circle) and 3.2 mL/min (triangle).

In the experiments conducted without a liquid flow, the temperature exhibits a non-linear rise with increasing supply voltage. Comparing the measurements of an integrated sensor with those of a discrete sensor, we can see that the integrated sensor consistently records higher temperatures. The largest deviation occurred at a supply voltage of 7 V, with the integrated sensor recording 60 °C and the discrete sensor recording 53 °C. This deviation is to be expected as the integrated sensor measures the temperature of the LTCC structure, while the discrete sensor measures the temperature in a cavity filled with water.

Under flow conditions, the temperature trends remain analogous. However, it is noticeable that the temperature increases less at higher flow rates and the difference between the temperatures measured by the integrated and discrete sensors is smaller. This suggests that the liquid flow dampens the temperature rise and minimises the difference between the two sensor types.

3.4 Demonstration of potential applications: Electrochemical response

The MFS with the flow and temperature-control system and the corresponding electronics can serve as a miniature analytical device. We investigated the applicability of the MFS developed here as an electrochemical device by monitoring the electron transfer in the model redox system of HCF on commercially available SPEs at various flows and temperatures. Figure 8a shows an image of the open structure MFS with the SPE in a cavity to assist the reader with visualisation, while Figure 8 b shows the MFS with inlet and outlet ports, electrical connections for the heating elements and temperature sensors bonded to the contact pads, and the SPE with a connection for the electrochemical measurements.

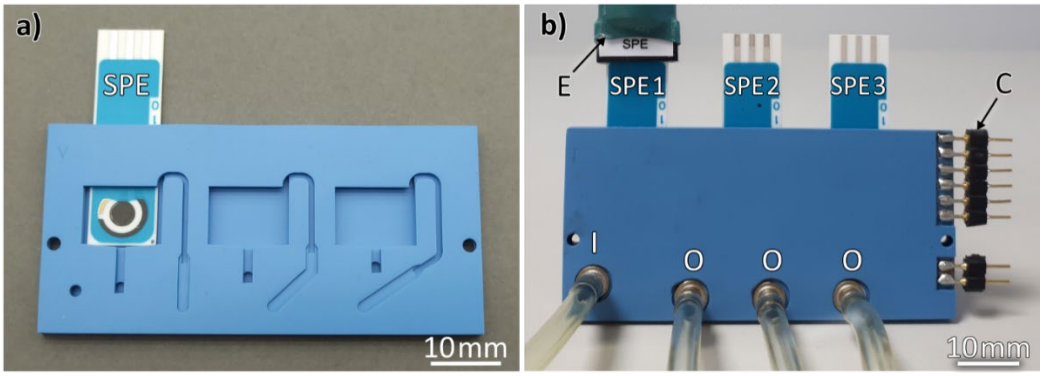

Figure 8: LTCC structure with SPE a) top view of the open structure; b) MFS with SPEs inserted in three cavities. SPE - screen-printed electrode; I - inlet port, O - outlet port, C - electrical connections; E - connector for electrochemical measurements.

As a starting point, cyclic voltammetry was performed in three different experimental setups, i.e., in our MFS, in a conventional electrochemical cell (CEC), and in a droplet (D), using identical SPEs, PBS, and HCF. Measurements were performed under identical conditions at 25 °C without a flow. The cyclic voltammograms are shown in Figure 9. The cyclic voltammograms of the PBS supporting electrolyte measured in three different setups were similar and gave similar capacitive currents. The values of the peak current obtained at 0 V were 0.06 μA, 0.07 μA and 0.10 μA for the measurements performed in the MFS, CEC and D, respectively. The voltammograms of the HCF displayed the characteristic peaks that are expected from this redox couple. As expected, the voltammograms of the HCF measured in the MC, CEC and D showed similar cathodic (i_{pc}) and anodic (i_{pa}) peak currents and similar peak-to-peak separation distances ΔE_{pp} (Table I). The results obtained in the three different experimental setups were consistent, confirming that CV measurements are relevant in the MFS. Additionally, they demonstrate that the developed MFS display the predicted behaviour at 25 °C under static conditions.

Table I: Characteristics of SPE voltammograms obtained in HFC solution

Set up	i_{pc}[mA]	i_{pa}[mA]	i_{pc}/i_{pa}	E_{pc}[V]	E_{pa} [V]	ΔE_{pp}[mV]
MS	-0.051	0.055	0.93	-0.171	0.371	542
CEC	-0.051	0.058	0.88	-0.176	0.361	537
D	-0.049	0.056	0.88	-0.154	0.364	518

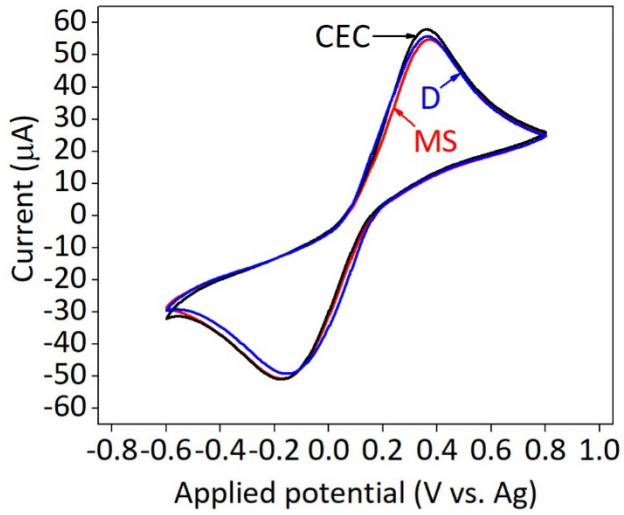

Figure 9: Cyclic voltammograms of SPE in PBS and in HCF measured in MFS, CEC and D set up at 25 °C.

Overlays of the characteristic cyclic voltammograms of SPE in HCF, measured in the MFS at different flow rates of 0, 1, 2, and 4 mL/min and a constant temperature of 25 °C, are shown in Figure 10a. The shape of the cyclic voltammograms changes when the flow is introduced into the MFS. All the experimental voltammograms exhibit some hysteresis between the forward and reverse scans. The hysteresis is most pronounced under static conditions. As expected, with increasing flow rate the hysteresis becomes narrower and acquires a more sigmoidal shape, which is due to the faster convective transport of the probe to the electrode surface and therefore a higher Faradic current is obtained [36–38]. As the flow rate increases, the hysteresis becomes narrower and takes on a more sigmoidal shape, which is ascribed to an enhanced physical process under flow [36,37]. The steady-state current (i_{ss}), i.e., the plateau current, increases with the increasing flow and is well defined at a flow rate of 4 mL/min.

Figure 10b shows the superposition of the characteristic voltammograms of the SPE in HCF, measured in the MFS at temperatures of 25, 35, and 45 °C and a constant flow of 4 mL/min. The shape of all curves is sigmoidal with hysteresis between the forward and reverse scans. The hysteresis becomes narrower at higher temperatures. The i_{ss} is well defined and increases with the increasing temperature. This is expected since the i_{ss} is linearly related to the number of electrons transferred in the reaction, the Faraday constant, the initial concentration of Fe^{2+}/Fe^{3+}, the dimensions of the working electrode and the diffusion coefficient of Fe^{2+}/Fe^{3+}, according to the Randles-Sevcik equation. Among these parameters only the diffusion coefficient depends on the temperature. It increases with the increasing temperature [39] and thus i_{ss}.

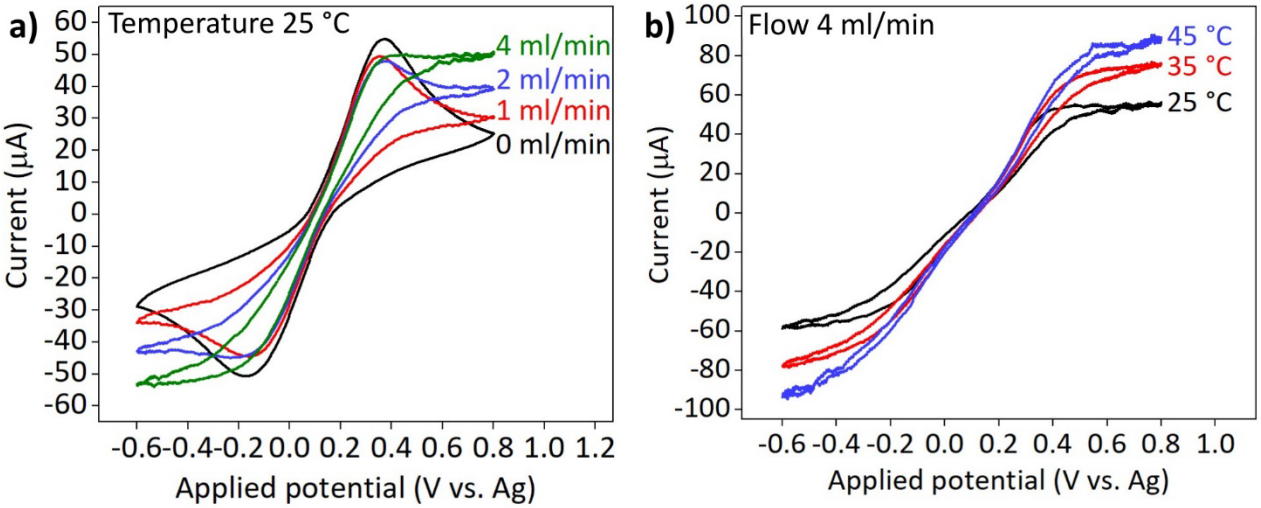

Figure 10: a) Cyclic voltammograms of the SPE in HCF measured in the MFS. a) at a flow of 0, 1, 2 and 4 mL/min and constant temperature 25°C; b) at temperatures 25, 35 and 45 °C and at a constant flow of 4 mL/min.

The CV measurements in the MFS under controlled flow and temperature show that a miniature fluidic system realised in LTCC and multilayer ceramic technology, in synergistic combination with commercially available SPEs, is suitable for a wide range of electrochemical applications. By tailoring the composition of the working electrode with specific nanoparticles or molecules such as metals, metal oxides or organic molecules, the system can be used for the identification of specific contaminants in water. Such investigations are traditionally carried out under stagnant conditions, i.e., in an electrochemical cell or with a drop of liquid applied to the SPE surface [40]. Therefore, future work should focus on measuring the EC response of the modified electrode under flow conditions and in particular its flow time stability. The knowledge gained from these results should be transferred to evaluations in model pollutant solutions as well as to real samples. The developed MFS provides convincing evidence that LTCC technology allows flexible design and the integration of electronic and fluidic components into the system. However, modelling the MFS architecture in relation to the fluidic and electronic components would be beneficial for improved flow

and temperature control in the EC measurements. Making well-defined and uniform channels and cavities will be a challenge with LTCC technology, thus each measurement location should be calibrated separately.

4 Conclusions

Previous studies have shown that microfluidic electrochemical sensors can detect various pollutants in aqueous environmental samples and are suitable for on-site analysis even in remote areas. However, a major limitation of these systems was the lack of temperature control during electrochemical measurements. This study aimed to address this limitation by developing a miniature fluidic system (MFS) with integrated heaters and temperature sensors, and fluidic elements such as cavities and channels. The MFS was made from low-temperature co-fired ceramic (LTCC) tapes, which were cut, laminated, and fired at 875°C. The resulting ceramic structure has three cavities that serve as measuring sites for easy insertion and replacement of electrochemical sensors, especially commercially available screen-printed electrodes (SPEs). The MFS also enables flow control using an external pump. In the experiments it was found that the developed MFS allows precise temperature control from room temperature to 125 °C and flow control up to 20 mL/min using an external pump. The comparable electrochemical responses of commercial SPEs in a typical redox probe solution in the MFS at room temperature and under stagnant conditions were the same as those obtained in conventional electrochemical cells and in the droplet. This agreement confirmed the accuracy of the measurements. In addition, the response was checked in the MFS for a flow of 4 mL/min and different temperatures (25 °C, 35 °C and 45 °C). The innovative MFS offers the possibility to detect various water pollutants quickly and easily, especially in remote areas and under controlled flow and temperature conditions. The system's potential for modification of the SPE working electrodes and to measure simultaneously the EC response at different measurement sites increases the applicability of the system in water-quality analysis. The use of LTCC ensures good mechanical properties, chemical stability, and resistance to high temperatures up to several hundred °C. This makes the ceramic MFS suitable for applications in areas where high temperatures and contact with aggressive chemicals are common. Possible areas of application include food processing, industrial real-time and environmental monitoring, energy management, aerospace, and the automotive industry.

Acknowledgments

The authors would like to acknowledge Mitja Jerlah for the fabricating multilayer ceramic structures.

Funding

This work was supported by the Slovenian Research and Innovation Agency [grant numbers P2-0105, J2-3049, P1-053, PR-11483].

CRediT authorship contribution statement

Danjela Kuscer: Conceptualization; Funding acquisition; Investigation; Methodology; Project administration; Resources; Supervision; Visualization; Roles/Writing - original draft; and Writing - review & editing.**Barbara Repič**: Investigation; Formal analysis; Visualization; Roles/Writing - original draft; **Kostja Makarovič**: Conceptualization, methodology; **Maksimiljan Dekleva**: Formal analysis; Writing – review & editing; **Gregor Marolt**: Supervision; Validation, Writing - review & editing; **Helena Prosen**: Funding acquisition; Project administration; Resources; Writing – review & editing; **Darko Belavič**: Conceptualization; Investigation; Visualization; Roles/Writing - original draft;

Declaration of Generative AI and AI-assisted technologies in the writing process

The authors did not use generative AI and AI-assisted technologies in the writing process.

5 References

[1] L. Lin, H. Yang, X. Xu, Effects of Water Pollution on Human Health and Disease Heterogeneity: A Review, Front. Environ. Sci. 10 (2022) 880246. https://doi.org/10.3389/fenvs.2022.880246.

[2] G. Daniele, B. Giroud, C. Jabot, E. Vulliet, Exposure assessment of honeybees through study of hive matrices: analysis of selected pesticide residues in honeybees, beebread, and beeswax from French beehives by LC-MS/MS, Environ. Sci. Pollut. Res. 25 (2018) 6145–6153. https://doi.org/10.1007/s11356-017-9227-7.

[3] G. Codling, Y. Al Naggar, J.P. Giesy, A.J. Robertson, Concentrations of neonicotinoid insecticides in honey, pollen and honey bees (Apis mellifera L.) in central Saskatchewan, Canada, Chemosphere. 144 (2016) 2321–2328. https://doi.org/10.1016/j.chemosphere.2015.10.135.

[4] L. Marle, G.M. Greenway, Microfluidic devices for environmental monitoring, TrAC Trends Anal. Chem. 24 (2005) 795–802. https://doi.org/10.1016/j.trac.2005.08.003.

[5] F.P. Pereira, Miniaturization in Sample Preparation, De Gruyter Open Poland, 2014. https://doi.org/10.2478/9783110410181.

[6] M. Akbari Kenari, E. Rezvani Ghomi, A. Akbari Kenari, S.M.S. Arabi, J. Deylami, S. Ramakrishna, Biomedical applications of microfluidic devices: Achievements and challenges, Polym. Adv. Technol. 33 (2022) 3920–3934. https://doi.org/10.1002/pat.5847.

[7] F. Sassa, G.C. Biswas, H. Suzuki, Microfabricated electrochemical sensing devices, Lab. Chip. 20 (2020) 1358–1389. https://doi.org/10.1039/C9LC01112A.

[8] Z. Li, H. Liu, D. Wang, M. Zhang, Y. Yang, T. Ren, Recent advances in microfluidic sensors for nutrients detection in water, TrAC Trends Anal. Chem. 158 (2023) 116790. https://doi.org/10.1016/j.trac.2022.116790.

[9] X. Liu, Y. Yao, Y. Ying, J. Ping, Recent advances in nanomaterial-enabled screen-printed electrochemical sensors for heavy metal detection, TrAC Trends Anal. Chem. 115 (2019) 187–202. https://doi.org/10.1016/j.trac.2019.03.021.

[10] J.F. Tan, A. Anastasi, S. Chandra, Electrochemical detection of nitrate, nitrite and ammonium for on-site water quality monitoring, Curr. Opin. Electrochem. 32 (2022) 100926. https://doi.org/10.1016/j.coelec.2021.100926.

[11] C. Jiang, Y. He, Y. Liu, Recent advances in sensors for electrochemical analysis of nitrate in food and environmental matrices, Analyst. 145 (2020) 5400–5413. https://doi.org/10.1039/D0AN00823K.

[12] I.G. Munteanu, C. Apetrei, A Review on Electrochemical Sensors and Biosensors Used in Assessing Antioxidant Activity, Antioxidants. 11 (2022) 584. https://doi.org/10.3390/antiox11030584.

[13] P.A. Raymundo-Pereira, T.A. Silva, F.R. Caetano, L. Ribovski, E. Zapp, D. Brondani, M.F. Bergamini, L.H. Marcolino, C.E. Banks, O.N. Oliveira, B.C. Janegitz, O. Fatibello-Filho, Polyphenol oxidase-based electrochemical biosensors: A review, Anal. Chim. Acta. 1139 (2020) 198–221. https://doi.org/10.1016/j.aca.2020.07.055.

[14] S.A.A. Almeida, E. Arasa, M. Puyol, C.S. Martinez-Cisneros, J. Alonso-Chamarro, M.C.B.S.M. Montenegro, M.G.F. Sales, Novel LTCC-potentiometric microfluidic device for biparametric analysis of organic compounds carrying plastic antibodies as ionophores: Application to sulfamethoxazole and trimethoprim, Biosens. Bioelectron. 30 (2011) 197–203. https://doi.org/10.1016/j.bios.2011.09.011.

[15] N. Lezi, A. Economou, Voltammetric Determination of Neonicotinoid Pesticides at Disposable Screen-Printed Sensors Featuring a Sputtered Bismuth Electrode, Electroanalysis. 27 (2015) 2313–2321. https://doi.org/10.1002/elan.201500127.

[16] R. Umapathi, S.M. Ghoreishian, S. Sonwal, G.M. Rani, Y.S. Huh, Portable electrochemical sensing methodologies for on-site detection of pesticide residues in fruits and vegetables, Coord. Chem. Rev. 453 (2022) 214305. https://doi.org/10.1016/j.ccr.2021.214305.

[17] J. Kudr, O. Zitka, M. Klimanek, R. Vrba, V. Adam, Microfluidic electrochemical devices for pollution analysis–A review, Sens. Actuators B Chem. 246 (2017) 578–590. https://doi.org/10.1016/j.snb.2017.02.052.

[18] J. Ganesamurthi, M. Keerthi, S.-M. Chen, R. Shanmugam, Electrochemical detection of thiamethoxam in food samples based on Co3O4 Nanoparticle@Graphitic carbon nitride composite, Ecotoxicol. Environ. Saf. 189 (2020) 110035. https://doi.org/10.1016/j.ecoenv.2019.110035.
[19] N. Ibáñez-García, J. Alonso, C.S. Martínez-Cisneros, F. Valdés, Green-tape ceramics. New technological approach for integrating electronics and fluidics in microsystems, TrAC Trends Anal. Chem. 27 (2008) 24–33. https://doi.org/10.1016/j.trac.2007.11.002.
[20] J.M. Mohan, K. Amreen, A. Javed, S.K. Dubey, S. Goel, Emerging trends in miniaturized and microfluidic electrochemical sensing platforms, Curr. Opin. Electrochem. 33 (2022) 100930. https://doi.org/10.1016/j.coelec.2021.100930.
[21] J. Varghese, N. Joseph, H. Jantunen, Multilayer Glass–Ceramic/Ceramic Composite Substrates, in: M. Pomeroy (Ed.), Encycl. Mater. Tech. Ceram. Glas., Elsevier, Oxford, 2021: pp. 437–451. https://doi.org/10.1016/B978-0-12-818542-1.00026-6.
[22] K. Malecha, L.J. Golonka, Microchannel fabrication process in LTCC ceramics, Microelectron. Reliab. 48 (2008) 866–871. https://doi.org/10.1016/j.microrel.2008.03.013.
[23] M.J. Czok, R.J. Tadaszak, P.I. Bembnowicz, L.J. Golonka, LTCC based chip for monitoring in biological applications, Sens. Actuators B Chem. 189 (2013) 118–122. https://doi.org/10.1016/j.snb.2013.01.085.
[24] D. Jurków, T. Maeder, A. Dąbrowski, M.S. Zarnik, D. Belavič, H. Bartsch, J. Müller, Overview on low temperature co-fired ceramic sensors, Sens. Actuators Phys. 233 (2015) 125–146. https://doi.org/10.1016/j.sna.2015.05.023.
[25] M. Goldbach, H. Axthelm, M. Keusgen, LTCC-based microchips for the electrochemical detection of phenolic compounds, Sens. Actuators B Chem. 120 (2006) 346–351. https://doi.org/10.1016/j.snb.2006.01.047.
[26] A. Vasudev, A. Kaushik, Y. Tomizawa, N. Norena, S. Bhansali, An LTCC-based microfluidic system for label-free, electrochemical detection of cortisol, Sens. Actuators B Chem. 182 (2013) 139–146. https://doi.org/10.1016/j.snb.2013.02.096.
[27] Y. Imanaka, Multilayered Low Temperature Cofired Ceramics (LTCC) Technology, 1st ed., Springer New York, New York, 2005. https://doi.org/10.1007/b101196.
[28] J. Haber, B. Jiang, T. Maeder, N. Borhani, J. Thome, A. Renken, L. Kiwi-Minsker, Intensification of highly exothermic fast reaction by multi-injection microstructured reactor, Chem. Eng. Process. Process Intensif. 84 (2014) 14–23. https://doi.org/10.1016/j.cep.2014.02.007.
[29] A. Brandenburg, J. Kita, A. Groß, R. Moos, Novel tube-type LTCC transducers with buried heaters and inner interdigitated electrodes as a platform for gas sensing at various high temperatures, Sens. Actuators B Chem. 189 (2013) 80–88. https://doi.org/10.1016/j.snb.2012.12.119.
[30] J.O. Bockris, A.K.N. Reddy, Modern Electrochemistry 2B: Electrodics in Chemistry, Engineering, Biology and Environmental Science, 2nd Edition, Springer, New York, 2001.
[31] M.H. Miles, G. Kissel, P.W.T. Lu, S. Srinivasan, Effect of Temperature on Electrode Kinetic Parameters for Hydrogen and Oxygen Evolution Reactions on Nickel Electrodes in Alkaline Solutions, J. Electrochem. Soc. 123 (1976) 332. https://doi.org/10.1149/1.2132820.
[32] Y. Zong, P. Chakthranont, J. Suntivich, Temperature Effect of CO2 Reduction Electrocatalysis on Copper: Potential Dependency of Activation Energy, J. Electrochem. Energy Convers. Storage. 17 (2020) 041007. https://doi.org/10.1115/1.4046552.
[33] G.G. Wildgoose, D. Giovanelli, N.S. Lawrence, R.G. Compton, High-Temperature Electrochemistry: A Review, Electroanalysis. 16 (2004) 421–433. https://doi.org/10.1002/elan.200302875.
[34] D. Belavic, A. Bradeško, H. Uršič, The investigation of basic microfluidic elements in LTCC structures, Microelectron. Int. 35 (2018) 133–138. https://doi.org/10.1108/MI-12-2017-0072.
[35] M. Hrovat, D. Belavič, J. Kita, J. Holc, J. Cilenšek, S. Drnovšek, Thick-film NTC thermistors and LTCC materials: The dependence of the electrical and microstructural characteristics on the firing temperature, J. Eur. Ceram. Soc. 29 (2009) 3265–3271. https://doi.org/10.1016/j.jeurceramsoc.2009.05.019.

[36] C.M. Gabardo, R.C. Adams-McGavin, O.M. Vanderfleet, L. Soleymani, Rapid prototyping of microfluidic devices with integrated wrinkled gold micro-/nano textured electrodes for electrochemical analysis, Analyst. 140 (2015) 5781–5788. https://doi.org/10.1039/C5AN00774G.
[37] Q. Chen, K. McKelvey, M.A. Edwards, H.S. White, Redox Cycling in Nanogap Electrochemical Cells. The Role of Electrostatics in Determining the Cell Response, J. Phys. Chem. C. 120 (2016) 17251–17260. https://doi.org/10.1021/acs.jpcc.6b05483.
[38] J. Nikolic, E. Expósito, J. Iniesta, J. González-Garcia, V. Montiel, Theoretical Concepts and Applications of a Rotating Disk Electrode, J. Chem. Educ. 77 (2000) 1191. https://doi.org/10.1021/ed077p1191.
[39] Y. Wang, E.I. Rogers, R.G. Compton, The measurement of the diffusion coefficients of ferrocene and ferrocenium and their temperature dependence in acetonitrile using double potential step microdisk electrode chronoamperometry, J. Electroanal. Chem. 648 (2010) 15–19. https://doi.org/10.1016/j.jelechem.2010.07.006.
[40] W. Duekhuntod, C. Karuwan, A. Tuantranont, D. Nacapricha, S. Teerasong, A Screen Printed Graphene Based Electrochemical Sensor for Single Drop Analysis of Hydroquinone in Cosmetic Products, Int. J. Electrochem. Sci. 14 (2019) 7631–7642. https://doi.org/10.20964/2019.08.94.

Supporting Information

An advanced miniature fluidic system in multilayer ceramic technology with precise temperature and flow control for *in situ* pollution monitoring

Danjela Kuscer[1,2*], Barbara Repič[1,2], Kostja Makarovič[1,4,5], Maksimiljan Dekleva[3], Gregor Marolt[3], Helena Prosen[3], Darko Belavič[1]

[1]Jožef Stefan Institute, Electronic Ceramics Department, Jamova cesta 39, Ljubljana, Slovenia

[2]Jožef Stefan International Postgraduate School, Jamova cesta 39, Ljubljana, Slovenia

[3] University of Ljubljana, Faculty of Chemistry and chemical technology, Večna pot 113, Ljubljana, Slovenia

4 KEKO-Oprema d.o.o., Grajski trg 15, Žužemberk, Slovenia

5 CoE NAMASTE, Jamova cesta 39, Ljubljana, Slovenia

*corresponding author: danjela.kuscer@ijs.si

S 1 Flow resistance R_h

A flow resistance (R_h) was calculated based on the Equation 1:

$$R_h \approx \frac{12 \cdot \mu \cdot L}{W \cdot H^3 (1 - 0.63\frac{H}{W})} \quad valid\ when\ H < W$$

R_h - flow resistance [Pa.s/m^3]
μ - Dynamic viscosity [Pa.s]
L - Length of the microchannel [m]
W - Width of the microchannel [m]; rectangular cross-section
H - Height of the microchannel [m]; rectangular cross-section

The R_h depends on the geometry of the channels and viscosity of the liquid. The geometry of the channels 1, 2, and 3 in the current MFMES

S are different and thus the corresponding R_h. Since the viscosity of the fluid (in our case water) decreases with the increasing temperature, the R_h also decreases with the increasing temperature. The R_h calculated for different temperatures in cavities 1, 2, and 3 are listed in the Table S1.

The flow of the fluid in the MFS was controlled by external pump. The pressure difference depends on the R_h and flow (Q) according to the Equation 2:

$$\Delta P = R_h \cdot Q$$

For example, the flow resistance at a temperature of 25 °C through cavities 1, 2, and 3 was 350, 353, and 325 MPa·s/m^3, respectively. Due to the different hydrodynamic resistances, the total input flow is divided through cavities 1, 2 and 3 in the ratio of 32.5%, 32.3% and 35.1%, respectively. We can see that the flow in cavity 3 is slightly higher compared to 1 and 2. If we compare the Rh at 25 and 20°C, we can see that the Rh is larger at 20°C than at 25°C, namely for about 13%. On the other hand, it is lower for about 55% at 70°C compared the one at 25°C. According to the Equation 2 this means that at a constant flow rate, set by external pump, the pressure difference is larger for about 13% at 20°C and smaller for about 55% at 70 °C.

Table S1: Viscosity of water and flow resistance R_h in cavity 1, 2 and 3 at different temperatures

Temperature	20 °C	25 °C	30 °C	35 °C	40 °C	45 °C	70°C
Viscosity [mPa.s]	1.0016	0.8900	0.7972	0.7191	0.6527	0.5958	0.4035
R_h in Cavity 1 [MPa.s/m^3]	393	350	313	282	256	234	158
R_h in Cavity 2 [MPa.s/m^3]	398	353	316	285	259	236	160
R_h in Cavity 3 [MPa.s/m^3]	366	325	291	263	239	218	147

In our experimetns, we set the flow rate with an external pump. For example, the R_h in cavity 1 at 25°C and 45°C, were 350 and 234 MPas/m^3, respectively. At a flow of 4 ml/min, the ΔP were 23 Pa and 15.6 Pa at 25 and 45°C, respectively.